International Journal of Biological Macromolecules 323 (2025) 147126

Contents lists available at ScienceDirect

International Journal of Biological Macromolecules

journal homepage: www.elsevier.com/locate/ijbiomac

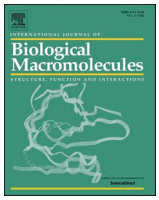

Chitosan/halloysite clay mixture for preservation of waterlogged archaeological woods

M.R. Caruso [a], G. D'Agostino [a,b], G. Cavallaro [a,*], O. Gómez-Laserna [c], M. Maguregui [d], G. Lazzara [a]

[a] Department of Physics and Chemistry "Emilio Segrè", Università degli Studi di Palermo, Viale delle Scienze, Ed. 17 "Stanislao Cannizzaro", 90128 Palermo, Italy
[b] Dipartimento di Scienze dell'Antichità, Università degli Studi di Roma "La Sapienza", 00185 Roma, Italy
[c] Department of Analytical Chemistry, Faculty of Science and Technology, University of the Basque Country UPV/EHU, P.O. Box 644, 48080 Bilbao, Spain
[d] Department of Analytical Chemistry, Faculty of Pharmacy, University of the Basque Country UPV/EHU, P.O. Box 450, 01008 Vitoria-Gasteiz, Spain

ARTICLE INFO

Keywords:
Archaeological wood
Conservation
Chitosan
Halloysite clay nanotubes
DMA

ABSTRACT

This work presents a sustainable protocol for the preservation of waterlogged archaeological wood (AW) by mixing chitosan (Chit) with halloysite clay nanotubes (HNTs). The conservation treatment is based on AW immersion within Chit/HNTs aqueous mixtures at variable composition. Surface characteristics of the treated wooden samples have been studied by colorimetric and microscopic techniques. Chemical elemental imaging shows the influence of the consolidation efficiency on the distribution of chitosan and clay inside the AW structure. The filling by chitosan/halloysite mixture generates improvements on the thermal and mechanical properties of archaeological woods. Besides, the treatment is efficient for wood preservation as demonstrated by aging tests under oxidative and acidic conditions. This paper demonstrates that the combination of chitosan polymer and halloysite clay nanotubes represents a promising alternative for conservation of waterlogged archaeological wood.

1. Introduction

Sustainable materials, such as biopolymers and natural nanofillers, have been pursued across a wide range of applications, including conservation of Cultural Heritage, due to environmental issues and a growing emphasis on health care [1–4]. Many traditional conservation methods involve the use of synthetic chemicals, such as organic solvents and polymers, which may have long-term environmental consequences causing health risks to conservators. Researchers are increasingly turning to sustainable and biodegradable materials, which include biopolymers (chitosan, pectin, cellulose derivatives) and natural nanomaterials, such as nanoclays and nanocellulose that offer effective conservation properties without environmental and health risks associated with traditional chemicals [5–7]. These natural materials are more compatible with the long-term preservation of fragile artifacts reducing the risk of damage caused by chemical reactions or environmental degradation over time [6,8,9].

In the conservation of waterlogged archaeological wood (AW), the preservation of the integrity of the wooden structure and the historical value is crucial [10]. AW is often fragile due to prolonged exposure to environmental factors, such as water, microorganisms, and soil conditions, which degrade its original composition. This degradation weakens the wood's cellular structure, making it prone to damage if not properly treated. Conservation methods aim to stabilize the wood and prevent further deterioration, while retaining as much of its original material as possible [11]. A significant challenge in conserving AW, particularly from underwater sites, is its waterlogged state. When wood becomes saturated with water over long periods, it loses its structural strength. If the water is allowed to evaporate too quickly, the wood can shrink, crack, or even disintegrate entirely. Thus, conservation techniques often focus on replacing water within the wooden structure with more stable substances to prevent these issues [12,13]. In recent years, the use of biopolymers reveals promising in conservation of Cultural Heritage, including waterlogged archaeological woods. Biopolymers and halloysite clay nanotubes (HNTs) are being explored for their ability to penetrate and reinforce the wood's structure at a molecular level [14]. These treatments aim to enhance both the physical stability of the wood and its resistance to biological degradation minimizing visual and

* Corresponding author.
E-mail address: giuseppe.cavallaro@unipa.it (G. Cavallaro).

https://doi.org/10.1016/j.ijbiomac.2025.147126
Received 29 April 2025; Received in revised form 23 July 2025; Accepted 24 August 2025
Available online 25 August 2025

chemical alterations occurring using some traditional methods [15]. One of the traditional method involves the use of polyethylene glycol (PEG), a water-soluble polymer that infiltrates the wood's structure and replaces the water within its cells, supporting them and preventing the dramatic shrinkage that would occur if the wood naturally dried [16,17]. HNTs loaded with calcium hydroxide was studied as alkaline fillers for the deacidification of AW combined with poly-ethylene-glycol (PEG). Mechanical investigations showed the deacidification action of HNTs with $(CaOH)_2$ on treated wood [18]. Pickering emulsions based on wax and halloysite nanotubes was used as sustainable protocol for the treatment of archaeological woods by using a biocompatible and sustainable system capable to protect and enhance mechanical properties of the wood [19]. Beeswax-halloysite nanocomposites were used to consolidate and improve thermal and mechanical properties of AW [20]. It is reported that the combination of cellulose and lignin at nano-scale can be employed for AW consolidation [21]. Due to their biocompatibility [22,23], halloysite clay nanotubes can be used for preservation of artworks. Recent literature reports that HNTs are versatile nanomaterials suitable for numerous technological applications, ranging from catalysis [24–27], packaging [28,29] and remediation [30–34]. Moreover, HNTs present low-toxicity leading to their use for biomedical and pharmaceutical purposes [35–39]. The combination of HNTs with chitosan biopolymer was explored to obtain functional composite materials useful for tissue engineering [40–42], oil spill remediation [32] and drug delivery [43–45]. Chitosan is an antimicrobial and antioxidant polymer that can be employed to obtain hydrogels for Cultural Heritage conservation [46,47] and controlled delivery [48–50]. In this work, we explored Chit/HNTs dispersions at different concentrations of nanoclays for the treatment of waterlogged archeological woods. We hypothesized that the interactions between chitosan and halloysite can favor the penetration of both carbohydrate and clay nanotubes within the wooden structure driving to improve its integrity and conservation state. Optical, colorimetric and elemental chemical imaging studies by micro energy dispersive X-Ray Fluorescence spectrometry (μ-ED-XRF) allowed us to understand the physico-chemical distribution of the composite on the wood and to assess the degree of colour variation after the treatment. Thermogravimetric analysis was crucial to study the thermal stability of untreated and treated wood samples. Treatment efficacy was correlated to their mass variations before and after the treatment. Both water vapor adsorption tests and aging experiments under acid environment demonstrated that Chit/HNTs dispersions are efficient for conservation of waterlogged archeological woods.

2. Experimental section

2.1. Materials

Chitosan (Chit), Acetic Acid (CH_3COOH) and Sodium chloride (NaCl, ≥99 %) are Sigma–Aldrich products. Based on Raman spectroscopy, we determined that the deacetylation degree (DD) of chitosan is 82 ± 2 %. The Raman spectrum of chitosan is reported in Supplementary Materials (Fig. S1). According to literature [51], the DD value was calculated by considering the intensity bands associated with the partial acetylation of the NH_2 group of chitosan. Further characterizations of pristine chitosan were performed by rheological measurements through shear-viscosity and frequency sweep tests (see Supplementary material). The determination of the intrinsic viscosity allowed us to estimate the molecular mass (242 ± 30 kDa) of chitosan. The flow curve of 2 wt% chitosan dispersed in acetic acid (0.5 wt%) solution was fitted by Cross model [52] allowing us to determine a zero-shear viscosity of 4.66 Pa•s. The terminal relaxation time (0.125 s) of chitosan was estimated by the inverse of the angular frequency at the crossover point between storage and loss moduli.

Halloysite nanotubes (HNTs) are a gift from I-Minerals Inc. The waterlogged archaeological woods are from the ship Chretienne C (II century, BC) discovered over the coast of Provence and kindly provided by Prof. Patrice Pomey from CNRS, Universite' de Provence (France). According to the procedure of the Italian standard (UNI 11205:2007), the archaeological woods were identified as *Pinus*. The identification was conducted in our previous work by optical microscopy on thin sections along the three characteristic directions of wood and subsequent comparison with taxonomic tables [53]. The waterlogged archaeological wood is identified as softwood with a cell wall density of 1.38 g cm^{-3} and high porosity (88–90 %) due to biological and chemical degradation causing the depolymerization of cellulosic matrix [54].

Based on the gravimetric method, we calculated the water content (76 wt%) of the waterlogged archaeological wood using the following equation:

$$\text{Water content} = \left(m_i - m_f\right)/m_i \cdot 100 \quad (1)$$

where m_i and m_f are the masses of wet and dried woods, respectively. The dehydration of the wood was performed at 105 °C as reported elsewhere [55].

According to literature [56,57], the degradation state of the archaeological wood was evaluated by the Maximum Water Content (MWC), which was determined as

$$\text{MWC} = \left(m_i - m_f\right)/m_f \cdot 100 \quad (2)$$

We detected that the MWC of the waterlogged archaeological wood is 335 %, which reflects an advanced stage of decay for the wooden structure that presents a rough and amorphous aspect. The latter was confirmed by optical and fluorescence images (Fig. 1) performed on thin sections of the AW sample. The micrographs show the presence of some signs of microbial attacks on the wooden structure.

2.2. Methods

2.2.1. Preparation of Chit/HNTs dispersions

Chitosan at concentration of 2 wt% was dispersed in 0.5 wt% acetic acid and it was magnetically stirred at 25 °C overnight until the complete polymer dissolution. Then, variable amounts of halloysite powder were added to the chitosan solution to systematically change the HNTs concentrations (0.2, 1, 2, and 3 wt%). The Chit/HNTs dispersions were magnetically stirred for 24 h to achieve the complete stabilization of the clay nanotubes. Chit/HNTs dispersions appeared creamy and homogeneous at room temperature. The preparation of Chit/HNTs mixtures is sketched in Fig. 2a.

2.2.2. Treatment of waterlogged archaeological wood

The AW was consolidated through the immersion method as described elsewhere [19,20]. The wood treatment is schematically represented in Fig. 2b. The untreated wood is indicated as AW_NT. The woods were kept in the Chit/HNTs dispersions for 72 h. For comparison, the wood was treated also by using a 2 wt% chitosan solution.

It should be noted that the dimensions of AW sample treated by chitosan/HNTs dispersions are ca. 2 × 2 × 1 cm (length, width, thickness). Three wood samples have been duplicated for each treatment. Before the immersion within the chitosan/HNTs mixtures, the AW was quickly dried with filter paper. Moreover, both the untreated and treated AW samples were kept within a desiccator under controlled conditions (temperature and relative humidity of 25 °C and 75 %, respectively) for 12 h before each testing except for the determination of the mass reductions upon drying.

The efficiency of the treatment was evaluated gravimetrically and by determining the mechanical performances of the treated wood samples. Preliminary investigations on the morphology of the treated woods were conducted by using a digital microscope (see Fig. S4 in Supplementary Materials). The treatment with pristine chitosan solution induced the formation of a thin polymeric layer on the surface of the waterlogged archaeological wood. Oppositely, the consolidation by chitosan/HNTs mixtures did not generate a superficial polymeric coating suggesting the

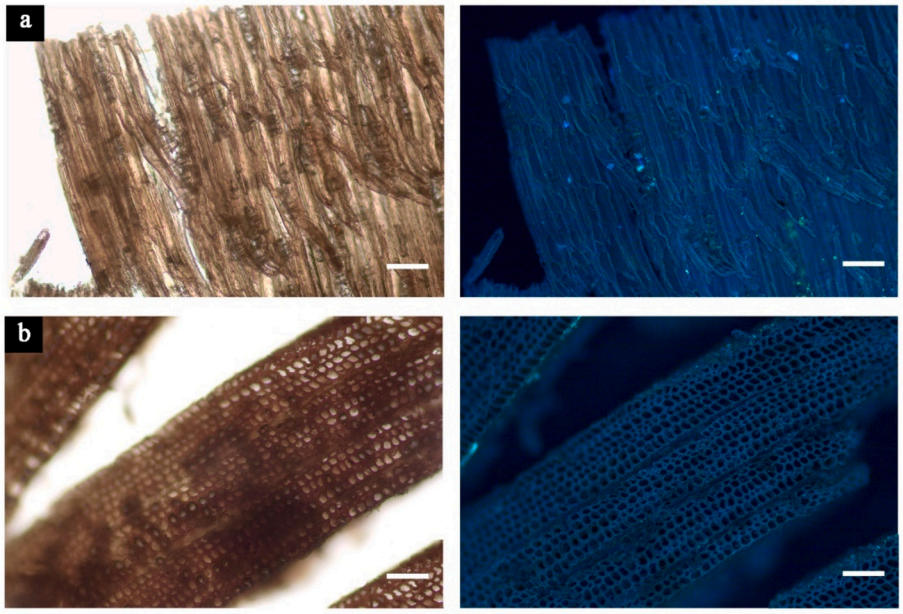

Fig. 1. Optical and fluorescence images of AW thin sections in tangential (a) and transverse (b) directions. The scale bar is 100 μm.

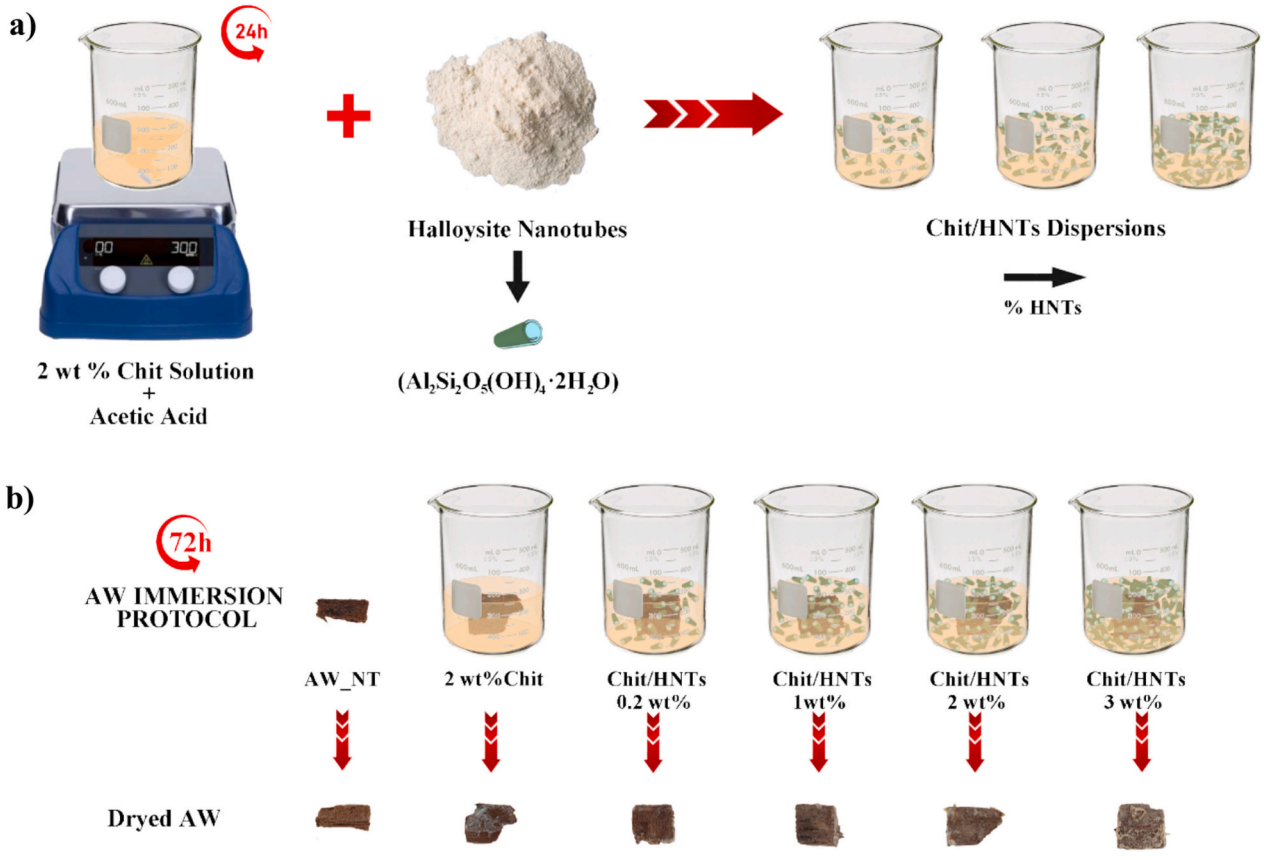

Fig. 2. Sketch for the preparation of Chit/HNT dispersion (a) and treatment protocol of waterlogged archaeological woods (b).

penetration of the consolidants (chitosan and halloysite) within the wooden structure.

2.2.3. Raman spectroscopy

Raman spectroscopy analysis was conducted using a Renishaw RA100 Raman microprobe spectrometer (Renishaw, Gloucestershire, UK) with a 785 nm excitation wavelength. Microscopic analysis was performed with a 20× long-range objective lens, mounted in the Raman microprobe head, which also featured a micro-video camera. Spectra were collected within the range of 100 to 3200 cm^{-1}, with an exposure time from 5 to 10 s per spectrum. To enhance the signal-to-noise ratio, each spectrum was accumulated five to ten times. The Raman

instruments were calibrated daily using the 520 cm^{-1} Raman band of a crystalline silicon chip. Spectral acquisition with the innoRam™ was carried out using BWSpec™ 3.26 software (B&WTEK INC). Spectral interpretation and data treatment were carried out using Fityk 1.3.1 Software.

2.2.4. Rheology

Rheological measurements were conducted using a rheometer (Discovery HR-2, TA Instruments, New Castle, DE, USA) equipped with a parallel plate (40 mm diameter, 1 mm gap). Shear-viscosity tests were performed in flow ramp mode, where the shear rate was progressively increased from 0.1 to 1000 s^{-1} over 60 s. The resulting flow curves (viscosity vs. shear rate) were analysed using the Cross equation [58]. Additionally, frequency sweep tests were carried out with a fixed strain amplitude of 1 % and an angular frequency range of 0.01 to 10 Hz to evaluate viscoelastic properties by determining the storage (G') and loss (G") moduli as functions of angular frequency.

2.2.5. Optical and fluorescence microscopies

Preliminary optical images were acquired by using a digital microscope, Dino-Lite 20×-200× (Olympus, Tokyo, Japan).

The morphology of the untreated and treated woods was also investigated through an optical microscope (NeXcope NE710, TiEsseLab), equipped with a digital camera (TiEsseLab MIchrome 20), allowing for a detailed description of the wooden structure of AW samples. In addition to optical micrographs, we obtained fluorescence images using a fluorescence apparatus with multi wavelength LED source (NeXcope FL 900C LED). The excitation and emission wavelengths were set at 330 and 385 nm, respectively.

2.2.6. μ-Energy dispersion X-ray fluorescence spectrometry

μ-ED-XRF spectrometry was employed to perform an elemental analysis of the untreated and treated AW samples. The M4 TORNADO ED-XRF spectrometer (Bruker Nano GmbH, Berlin, Germany) allows measuring at 1 mm (mechanical collimation) and down to 25 μm (poly-capillary lens) of lateral resolution. In this work its tube working between 10 and 50 kV and 100–600 μA and connected to a poly-capillary system that allows to work under a lateral/spatial resolution of 25 μm measured for Mo Kα (around 17 mm at 2.3 keV to 32 μm at 18.3 keV) was used. The detection of the fluorescence radiation was performed using an XFlash® silicon drift detector with 30 mm^2 sensitive area and energy resolution of 145 eV for Mn-Kα energy. To improve the detection of the lightest elements ($Z < 19$), measurements were acquired under vacuum (20 mbar). The spectral data acquisition and treatment was performed using the M4 TORNADO software. Two video microscopes were employed for the focusing process; the first examined the sample at a low magnification (1 cm^2 area), and the second carried out the final focusing (1 mm^2 area) to perform the analysis. A multi-point strategy was applied to measure halloysite nanotubes and chitosan. Concretely, 6 measurements were conducted directly on each wood sample. Moreover, apart from direct measurements, isolated HNTs powders obtained were also measured with the benchtop instruments acquired during 100 s.

Apart from single point measurements, the instrument was also used for imaging studies of the mineral samples, obtaining the distribution maps (hypermaps) of the elements detected. The mapping process took place at a 25 ms scan rate with a 20 μm step size. A prior deconvolution of the signals in the total spectrum representing the entire mapped area was carried out to create the elemental images. The distribution map of each element was then displayed as a function of each K_α line's intensity.

2.2.7. Thermogravimetric analysis

Thermogravimetric (TG) analyses were carried out using Q5000 IR apparatus (TA Instruments, New Castle, DE, USA) under N_2 atmosphere (gas flows of 25 and 10 $cm^3\,min^{-1}$ were employed for the sample and the balance, respectively). Each treated wood samples (ca. 3 mg) were heated from room temperature up to 600 °C with a scanning rate of 20 °C min^{-1}. The amount of the HNTs loaded in the wood was determined by using the rule of mixtures [18] for the degraded matters at 600 °C (MD_{600}), which was calculated for all samples as

$$MD_{600} = 100–(MR_{600} + ML_{150}) \quad (2)$$

where MR_{600} is the residual matter at 600 °C, while ML_{150} is the mass loss between 25 and 150 °C.

2.2.8. Colorimetric analysis

A colorimeter (NH300 Colorimeter, 3NH Shanghai Co., Ltd., China) with a spot size of 8 mm was used to measure colour parameters of treated and untreated AW samples. The device was calibrated using black and white plates. CQCS3 Software was used for data acquisition, a* (red-green), L* (lightness), and b* (yellow-blue) parameters, whiteness index (WI), yellowness index (YI) and total colour differences (ΔE) are measured for each treated wood samples and compared to untreated wood, L_0^*, a_0^*, b_0^*, by using the following equations:

$$YI = 142.86\ (b^*/L^*) \quad (3)$$

$$WI = 100–\sqrt{\left[(100–L^*)^2 + a^{*2} + b^{*2}\right]} \quad (4)$$

$$\Delta E = \sqrt{\left[(L^* - L_0{}^*)^2 + (a^* - a_0{}^*)^2 + (b^* - b_0{}^*)^2\right]} \quad (5)$$

2.2.9. Water uptake analysis

Treated and untreated wood samples were dried under vacuum at 25 °C for ca. 2 h until a constant weight was achieved. The water uptake (WU) experiments were carried out in a climate chamber containing saturated salt solutions of NaCl at 75 % relative humidity (RH%) and at temperature of 25.0 ± 0.5 °C. The samples were weighed (±0.00001 g) until constant weight. The WU% was calculated considering that M_0 and M_t are the masses of the sample before and after equilibration, respectively, through the equation.

$$WU\% = 100\cdot(M_t - M_0)/M_t \quad (6)$$

2.2.10. Water absorption by immersion test

Treated and untreated wood samples were dried under vacuum at 25 °C for ca. 2 h until constant weight. Samples were immersed in distilled water at temperature of 25.0 ± 0.5 °C and pH 7. The samples were weighed (±0.00001 g) until constant weight during the time. The WA% was calculated considering that M_0 and M_t the masses of the sample before and after equilibration, respectively, through the equation.

$$WA\% = 100\cdot(M_0–M_t)/M_0 \quad (7)$$

2.2.11. Dynamic-mechanical analysis

Dynamic Mechanical Analysis (DMA) was conducted on wood by a DMA Q800 apparatus (TA Instruments, New Castle, DE, USA) following stress vs strain at fixed temperature. It was used a compression clamp and working under a force ramp of 0.5 N min^{-1} to 15.0 N at 25.0 ± 0.5 °C. The mechanical performances for untreated and treated wood samples, before and after aging process, were determined by the analysis of stress vs strain curves on Universal Analysis software (TA Instruments), in terms of stress at breaking, and elastic modulus, calculated from the slope of the linear stress vs strain curves.

2.2.12. Fourier transform infrared spectroscopy

Fourier transform infrared (FTIR) studies were carried out through a Frontier FTIR spectrometer (PerkinElmer, Waltham, MA, USA) at room temperature. The spectra were recorded in the range between 4000 and 450 cm^{-1} with a 2 cm^{-1} spectral resolution from KBr pellets with a low content (< 2 wt%) of milled samples.

2.2.13. Aging experiments under oxidative and acidic conditions

Untreated and treated woods were placed in a closed desiccator saturated with nitric acid vapours at 25 °C. Specifically, the desiccator contained a Becher with HNO_3 solution (30 vol%) that guaranteed the saturation of the vapours. The aging time was fixed at 3 days. Prior to testing, all aged wood samples were re-equilibrated with ambient air for 30 days.

3. Results and discussions

3.1. Wood consolidation efficiency of Chit/HNTs dispersions

The consolidation efficiency of chitosan/HNTs dispersions was estimated by studying the mass reductions of untreated and treated wooden samples upon drying. Within this, it should be noted that the loss of wood is a key factor in assessing the structural stability of wooden archaeological artifacts as it influences their vulnerability to collapse during drying or under compression. As shown in Fig. 3, the mass reductions range between ca. 64–72 % for the woods consolidated with chitosan/halloysite at variable composition. As expected, these values are lower compared with that of the untreated wood (mass reduction of ca. 76 %) confirming the incorporation of halloysite and chitosan within the wooden structure.

The decrease of the mass reduction upon drying for archaeological woods treated with chitosan/HNTs reflects the partial filling of the wooden channels by both polymer and clay. Therefore, the treatment generates a reduction of the wood porosity reducing the volume that can be occupied by water. The increase of the HNTs concentration in the consolidating mixture decreased the wood mass reduction up to ca. 64 % highlighting an improvement of the consolidation efficiency, which leads the preservation of the structural integrity of the archaeological wooden samples. This finding highlighted that the enhancement of halloysite content in the consolidating mixture increases the amounts of consolidants (HNTs and chitosan) loaded within the wooden channels. Moreover, we can hypothesize that the presence of halloysite does not prevent the coating and the penetration of chitosan into the wood structure. Similar results were detected for archaeological woods treated by immersion with beeswax/HNTs [20] and polyethylene glycol/HNTs mixtures [18].

Microscopic observations of the treated woods (Fig. 4 and Fig. S5 in

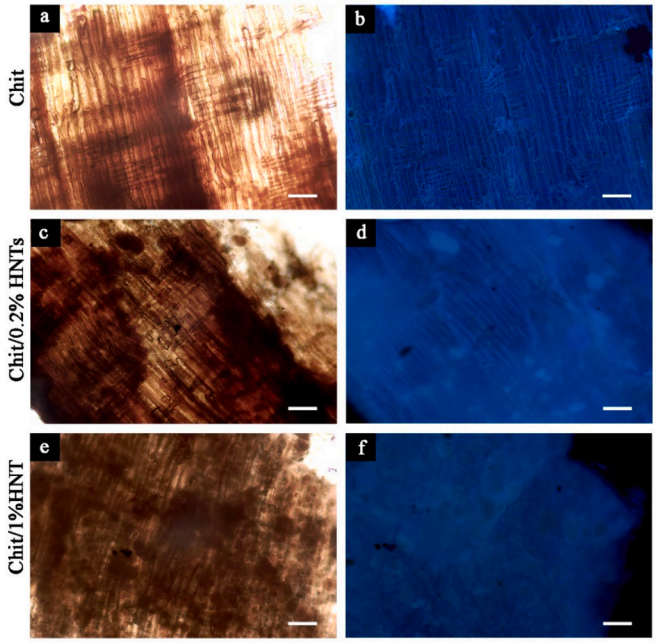

Fig. 4. Optical (a.c.e) and fluorescence (b,d,f) micrographs of thin sections in tangential direction of AW treated by chitosan solution and chitosan/HNTs mixtures at variable composition (0.2 wt% and 1 wt% of halloysite). The scale bar is 100 μm.

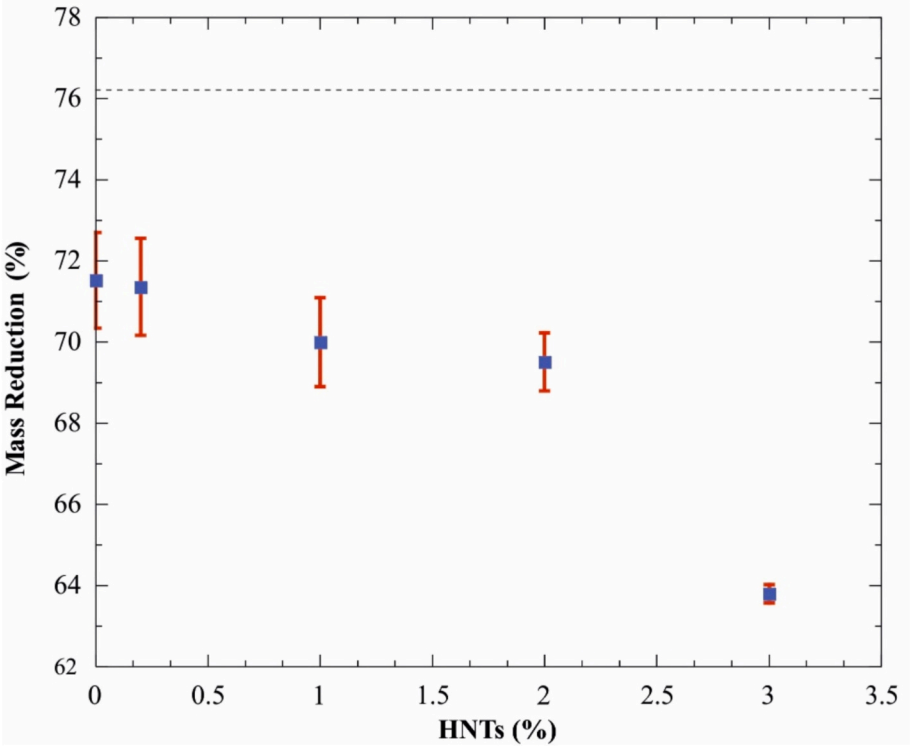

Fig. 3. Mass reduction upon drying of archaeological woods treated with chitosan/HNTs dispersions at variable halloysite concentration. The dashed line represents the mass reduction upon drying for untreated wood.

Supplementary Materials) confirmed that the consolidation efficiency is enhanced by increasing the HNTs amounts being that the porosity of the wooden structure was reduced. The wood samples treated with chitosan/HNTs mixtures (Figs. 4c-f) showed the presence of irregular microparticles that are formed by the clustering of halloysite clay nanotubes. The HNTs clusters can be incorporated inside the wood because they are smaller as compared with diameter of the wooden channels. On the other hand, AW treated with chitosan solution (Figs. 4a,b) evidenced that wooden channels are unfilled suggesting that pristine biopolymer is not efficient for consolidation, while it can be useful for coating protection.

3.2. Elemental mapping of archaeological woods consolidated by Chit/HNTs dispersions

The multi-point μ-ED-XRF spectrometry measurements can provide comprehensive evidence of the elemental composition in both untreated and treated wood samples [59–62]. Fig. 5 shows XRF spectra of wooden samples before and after the treatment with chitosan and chitosan/HNTs dispersions at variable composition.

As concerns untreated wood, the spectrum revealed the presence of sulphur (S), iron (Fe), potassium (K), calcium (Ca), copper (Cu), and titanium (Ti). In the multi-point study, we did not detect any traces of aluminium (Al) or silicon (Si) in the untreated samples. This finding could indicate that the wood did not contain both elements. Alternatively, their content could be under the limit of detection of the technique. In contrast, Al and Si were clearly observed in the samples treated with chit/HNTs mixtures. This confirms the effective deposition of HNTs on the wood surface. As evidenced in Supplementary Materials (Table S1), the concentration of Al and Si increased proportionally with the concentration of HNTs in the consolidating mixture. As these values were extracted using a fundamental parameters-base quantitative method that was not originally created for this kind of matrix, these numerical values are only indicative and not fully quantitative. As carbon (C), oxygen (O) and nitrogen (N) cannot be detected by ED-XRF, in principle chitosan, being derived from chitin, cannot be detected through this technique. However, chitosan used to treat the AW was separately analysed being possible to identify the presence of chlorine (Cl). Therefore, this element was used to determine the distribution of chitosan in the treated AW samples.

μ-ED-XRF spectrometry by means of an imaging strategy was also applied to evaluate the distribution of the target elements associated to chitosan (Cl) and HNTs (Al and Si) in the treated and untreated wood samples. The imaging study was useful to assess if Chit/HNTs dispersions were distributed homogeneously once wood samples were immersed. Although through multi-point study Al and Si were not detected, as it can be observed in Figs. 6b,c.

The imaging study (Fig. 6) allowed us to detect hot spots of Al and Si randomly distributed on the surface of untreated wood. As can be observed, the spatial distribution of Al and Si is highly reduced in the total area of the untreated wood scanned. On the contrary, these elements (associated to HNTs) are widely distributed on the surface of the treated wood samples. The distribution of HNTs appeared homogeneous on the surface of the wood samples, even at high concentrations of the nanotubes. The elemental mapping images in Fig. 6c revealed the presence of S, which is primarily associated with the untreated wood, in contrast to Al and Si. When the wood was treated with the Chit/HNTs dispersion, the spatial distribution of S decrease while HNTs cover the surface of the wood (see the combined elemental distribution maps of S, Al and S in Fig. 6c). As highlighted in Fig. 6c, the irregularities in the wood structure can influence the distribution of the HNTs (see Al and Si distribution maps in Fig. 6c). The distribution maps of Cl (see Fig. 6d) indicate that chitosan is uniformly distributed for all wooden samples.

3.3. Characterization of untreated and treated archaeological woods by thermogravimetry

According to literature [6,63,64], thermogravimetry represents a powerful tool to characterize waterlogged archaeological woods and evaluate the efficiency of consolidation protocols. Fig. 7a compares the thermogravimetric curves of pristine consolidants (chitosan and HNTs) and AW samples before and after the treatment with chitosan solution and chitosan/HNTs mixtures at variable composition. The corresponding differential thermogravimetric (DTG) curves are presented in Figs. 7b,c.

As a general result, we detected a mass loss at 25–150 °C that can be attributed to the water molecules physically adsorbed on the samples [65]. Then, the AW samples evidenced two clear mass reductions within the temperature interval of 180–380 °C and 380–500 °C, which can be related to thermal degradation of cellulosic components and lignin, respectively. The degradation steps of AW samples can be clearly discriminated by DTG curves, which presents two peaks in correspondence to thermal decompositions of cellulosic components and lignin (Fig. 7c). Regarding the untreated AW, we calculated a mass loss of 48.8

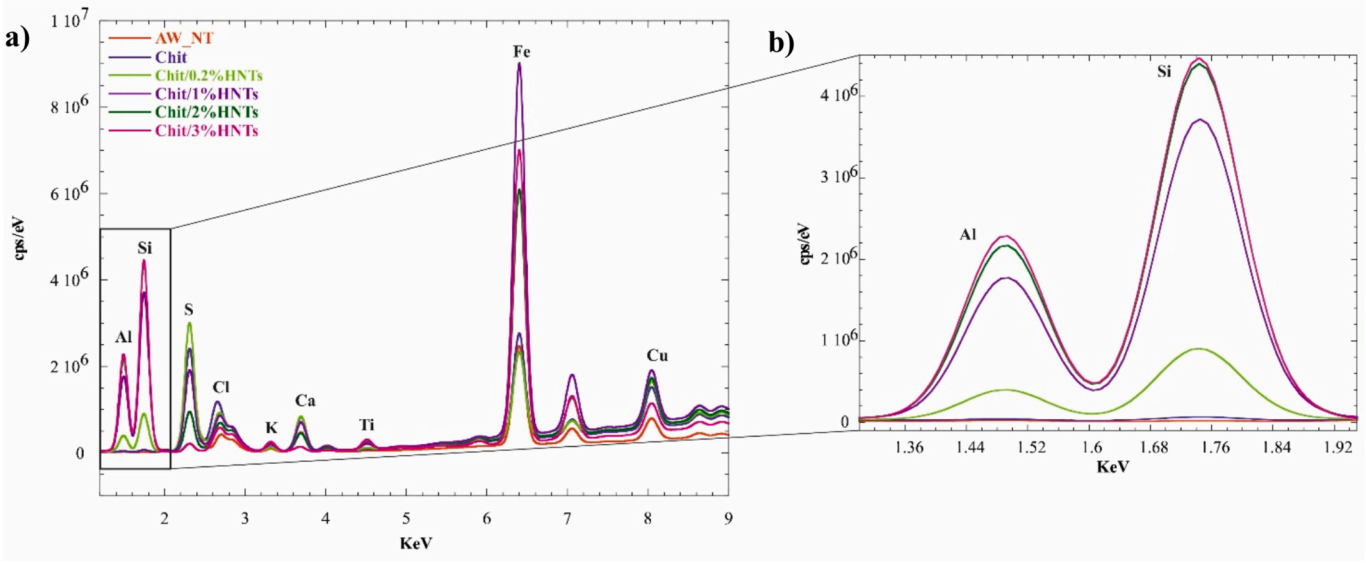

Fig. 5. a) XRF spectra of untreated and treated wood samples and b) magnification of Al and Si Kα lines.

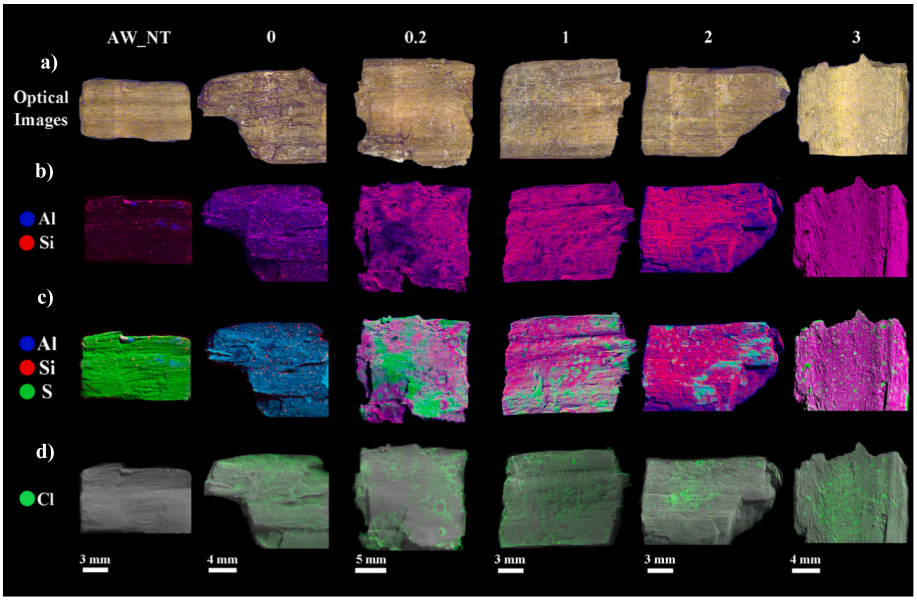

Fig. 6. a) Optical Images of untreated and treated wood samples. Elemental map images of b) Al—Si, c) Al-Si-S and d) Cl distribution on the surface of untreated and treated AW. Aluminium is in red, Silicon is in blue, Chlorine is in turquoise, and Sulphur is in green. Each column corresponds to various HNTs concentrations from 0 to 3 wt% and the untreated sample.

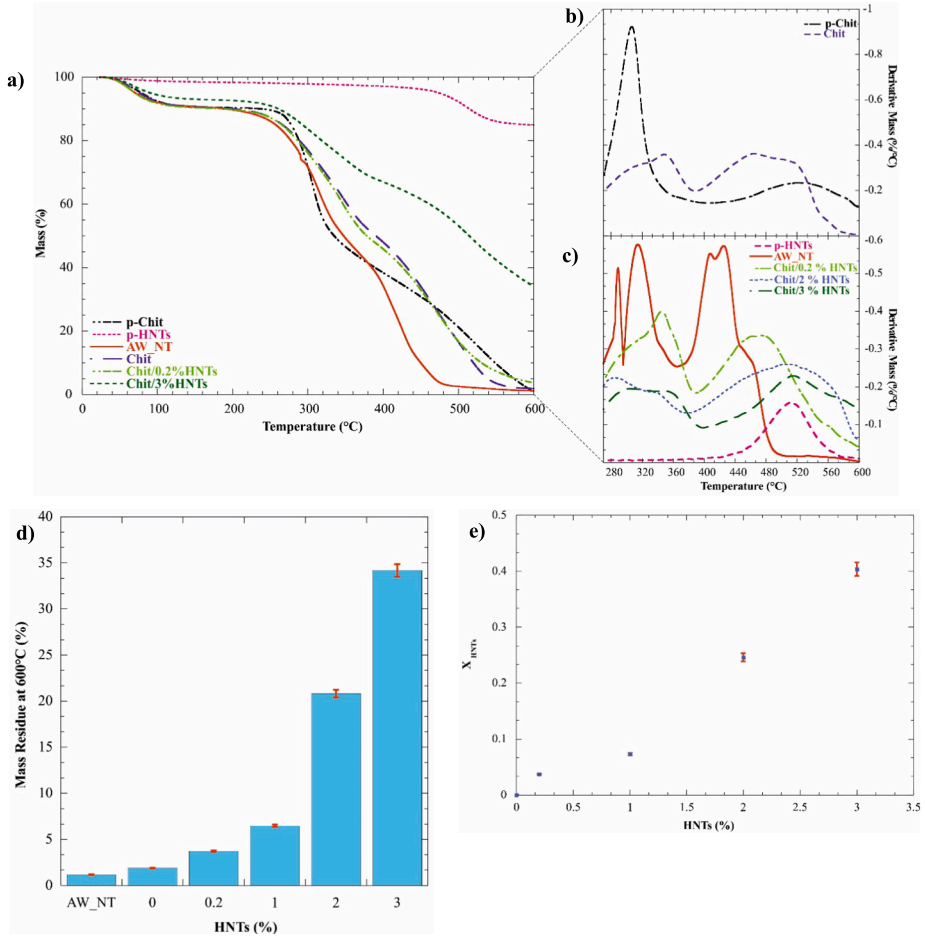

Fig. 7. Thermogravimetric (a) and Differential Thermogravimetric (b,c) curves of pure chitosan and HNTs, untreated wood and treated woods with Chit/HNTs at different concentrations of nanoclays. Residual mass at 600° of untreated and treated wood (d). Mass fraction of halloysite in the treated wood as a function of the HNTs concentration of the consolidating mixture (e).

% at 180–380 °C, while a mass reduction of 38.85 % was estimated at 380–500 °C. The ratio between these values reflects the composition of the wood in terms of cellulosic components and lignin. We estimated a cellulose/lignin mass ratio of 1.25, which is comparable to those of archaeological woods from different *taxa*, such as *Abies Alba* (1.39) [66] and *Quercus robur L.* (1.36–1.55) [67]. The specific cellulose/lignin composition cannot be determined for treated AW samples because chitosan degrades within the same temperature range. It should be noted that the chitosan degradation is associated to depolymerization and decomposition of polymeric chains, deacetylation and cleavage of glycosidic bonds and breakdown of the pyranose ring and residual carbon [68,69]. The overlap of thermal degradation for chitosan and wood components did not allow us to determine the amount of biopolymer entrapped in the wooden structure by thermogravimetry. Furthermore, we determined the residual matters at 600 °C (Fig. 7c) in order to estimate the composition of all samples in terms of inorganic and organic molecules. As expected, the residues at 600 °C are very low for untreated wood (1.18 wt%) and wood consolidated with pristine chitosan (1.90 wt %), while AW samples treated by chitosan/HNTs mixtures evidenced larger values (up to 35 wt%) in agreement with the entrapment of inorganic clay nanotubes within the wooden structure (Fig. 7c). Specifically, we observed that the residual mass at 600 °C is proportional to the amount of HNTs used for the wood consolidation.

It should be evidenced that the residue value at 600 °C of untreated AW reflects the presence of inorganic materials (ash and mineral components) encapsulated in wooden structure during the burial into the marine environment [55].

Due to the inorganic nature of clay nanotubes, the quantitative analysis of thermogravimetric data (Table S2 in Supplementary Materials) allowed us to determine the halloysite amounts entrapped in the woods treated with chitosan/HNTs dispersions using the rule of mixtures as reported elsewhere [18]. As displayed in Fig. 5d, the halloysite mass fraction (X_{HNTS}) shows an increasing trend with the HNTs concentration of the consolidating mixture. We determined that the wood consolidated with chit/HNTs 3 wt% contains ca. 40 wt% of halloysite highlighting a relevant capacity of clay nanotubes to penetrate within the wooden structure.

Furthermore, the analysis of thermogravimetric data allowed us to evaluate the effects of the consolidation on the thermal degradation of the AW components (cellulose and lignin). As shown by Figs. 5b,c, DTG peaks related to pyrolysis of AW cellulosic components (at ca. 300 °C for untreated wood) [70] are shifted to higher temperatures (ca. 360 °C) after treatment with chitosan and chitosan/HNTs dispersions. Moreover, the lignin decomposition (at ca. 420 °C before treatment) [71] occurred at higher temperature (from ca. 460 to 520 °C) after the consolidation protocol (Fig. 7b). Specifically, the DTG peaks of lignin degradation were centred at ca. 480, 500, and 520 °C for wooden samples treated with HNTs concentrations of 0.2, 2 and 3 wt%, respectively. Thermogravimetric results evidence that the AW consolidation by chitosan/HNTs composite promotes enhanced thermal stabilization effects on both lignin and cellulose with respect to those detected for pure chitosan. This finding agrees with the barrier action of clay nanotubes towards the thermal decomposition of organic macromolecules as reported elsewhere for polymer/HNTs nanocomposites [39,72,73].

3.4. Colorimetric properties of archaeological woods after treatment

Wooden samples were analysed by colorimetric analysis to evaluate visual changes caused by their immersion within chitosan/halloysite dispersions. Table 1 collects the colour parameters for all the investigated samples.

For all treated wood samples, we determine the total colour difference (ΔE) with the respect to pristine AW with the aim to quantitatively describe the influence of the consolidants (chitosan and chitosan/HNTs composites) on the colorimetric characteristics of the waterlogged archaeological wood. The treatment by chitosan solution induced a total colour difference (ΔE) of 5.14, which evidences slight colorimetric variations. The presence of HNTs (up to 2 wt%) in the consolidating dispersion did not determine significant ΔE variations being that the ΔE values range between 2.82 and 3.97, which correspond to negligible noticeable differences by the human eyes, as reported in the literature [74]. Similar results (ΔE = 2.5–3.8) were detected for AW treated by immersion in paraffin wax/HNTs Pickering emulsions at concentration of 0.5 wt% [19].

In contrast, the treatment with chitosan/HNTs mixture at the largest halloysite concentration (3 wt%) affected negatively the wood aspect with relevant colour changes as evidenced by the high ΔE value (14.09). The presence of small amounts of HNTs (0.2 wt%) in the consolidation protocol did not alter significantly white and yellow indexes (WI and YI), while opposite results were detected for larger HNTs concentrations. Indeed, the HNTs addition (from 1 wt%) in the consolidating formulations generated WI increases suggesting that the wood becomes whiter or more reflective to light. Moreover, we detected YI decreases that imply a reduction in yellowish tint, potentially making the wood appear brighter or less discoloured (Table 1).

3.5. Evaluation of hygroscopicity properties of wooden samples

The hygroscopicity of untreated and treated woods was evaluated through water uptake and immersion tests, to investigate the samples' ability to absorb water, either as vapor or liquid (Fig. 8a,b). In water uptake tests, wooden samples were exposed to a controlled atmosphere to measure their ability to absorb water vapor over time. The testing environment was maintained at a constant temperature of 25 °C with a relative humidity of 75 %. To ensure stable humidity levels, the chamber was saturated with a saturated NaCl solution, as described in the experimental section. The experiments were conducted for 14 days, and samples were weighed regularly to monitor any changes in their mass. This continuous monitoring allowed us to collect valuable data on the kinetics of water absorption ability of untreated and treated woods, leading for a better understanding of how quickly the wood reaches its hygroscopic equilibrium. For treated woods, we observed smaller mass variations and slower absorption rates compared to those of untreated wood (Fig. 8a). These effects are more relevant by increasing the HNTs concentration of the consolidating mixture. Accordingly, the can state that the water uptake data can be related to the filling degree of wooden channels. The water uptake at equilibrium (after 14 days) was reduced by ca. 35 % for the wood consolidation with chit/HNTs 3 wt%. In particular, we determined WU% values of ca. 12 % and ca. 7.5 % before and after treatment with chit/HNTs 3 wt%, respectively.

Table 1
Colorimetric parameters of untreated and treated archaeological woods.

HNTs (%)	L*	a*	b*	WI	YI	ΔE*
AW_NT	45.02 ± 0.10	11.25 ± 0.07	18.19 ± 0.04	40.99 ± 0.05	57.73 ± 0.01	
0	40.18 ± 0.2	11.82 ± 0.10	16.51 ± 0.06	39.82 ± 0.01	58.80 ± 0.12	5.14 ± 0.05
0.2	44.6 ± 0.2	12.57 ± 0.09	20.7 ± 0.1	39.51 ± 0.09	57.90 ± 0.01	2.87 ± 0.03
1	47.4 ± 0.2	9.83 ± 0.10	15.38 ± 0.03	44.36 ± 0.11	43.15 ± 0.07	3.97 ± 0.05
2	44.3 ± 0.2	11.91 ± 0.10	17.01 ± 0.04	41.13 ± 0.14	46.54 ± 0.06	2.82 ± 0.02
3	58.7 ± 0.3	8.00 ± 0.14	17.11 ± 0.08	54.56 ± 0.14	42.15 ± 0.01	14.09 ± 0.12

*Calculated with respect to untreated wood.

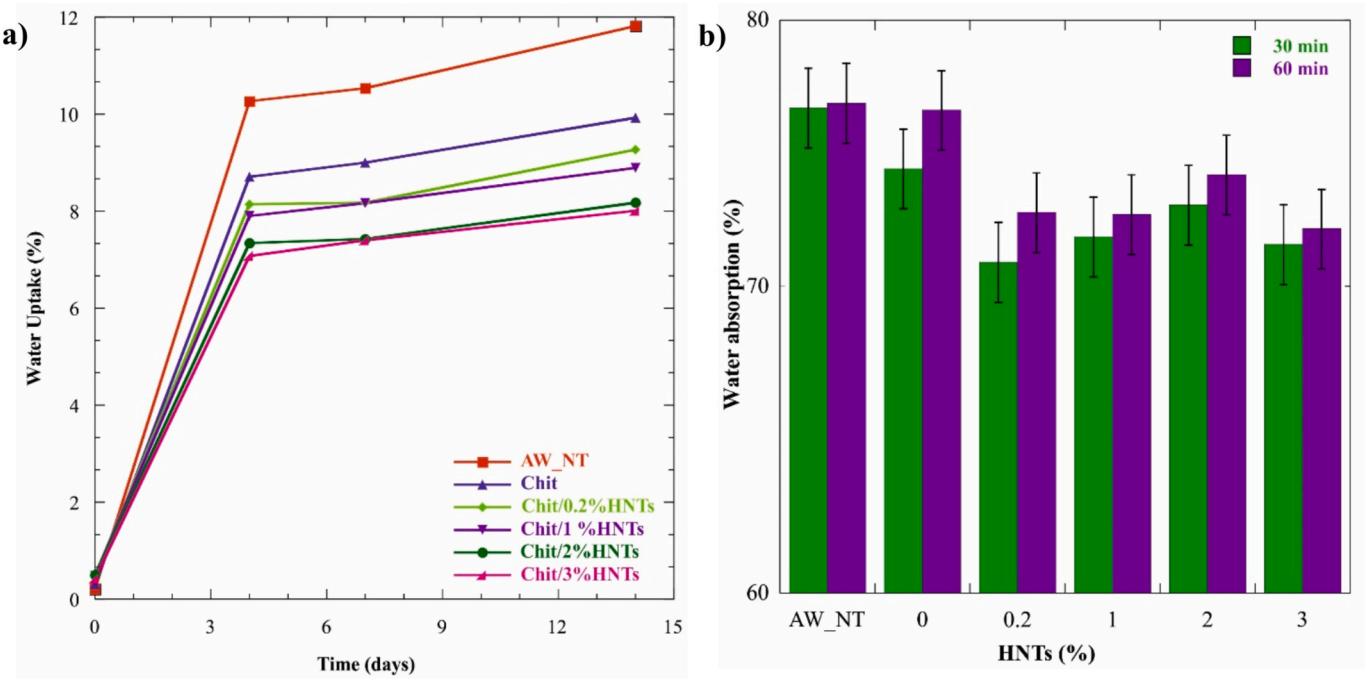

Fig. 8. a) Water Uptake values of untreated and treated wood samples at different times, 0, 4, 7 and 14 days. The error for water uptake data is ±0.1. b) Variation of mass of wood samples after water immersion test, measured in two times, 30 min and 60 min. Relative error for water uptake and water absorption data is 5 %.

Water immersion tests were carried out in a distilled water (pH = 7) for variable times (30 min, 1 h and 1 day). It should be noted that results after 1 day did not show any relevant differences compared to the variation mass after 1 h. Fig. 8b compares the water absorption data after 30 and 60 min. Untreated wood demonstrated the largest water absorption (WA%) values in agreement with its high porosity. This observation highlights the necessity for consolidation treatments to enhance archaeological wood's resistance to water, especially for preservation of Cultural Heritage.

Wood treated with chitosan showed a slight reduction in WA% after 30 min, while this effect is negligible after longer time. Chitosan's biopolymeric nature provides some degree of hydrophobicity due to its ability to form a thin film over the wood's surface. The slight WA% reduction suggests that pristine chitosan creates a coating protective layer on the wood surface, while it is not very efficient for consolidation and filling of wooden channels. The unchanged WA% after 1 h indicates that chitosan's protective barrier has limitations in slowing down water absorption over prolonged periods. On the other hand, the treatment by chitosan/HNTs mixtures induced significant WA% reductions confirming the capacity of halloysite clay nanotubes to penetrate the wooden structure decreasing the AW porosity. Namely, the combination of chitosan and HNTs guarantees the loading of consolidants inside the wooden channels that might lead to improvements of robustness and mechanical resistance of waterlogged archaeological wood.

3.6. Evaluation of the wood protection by chit/HNTs dispersions

The wood protection induced by the treatments with chitosan/halloysite mixtures was tested through Dynamic Mechanical Analysis (under compression mode) and monitoring lignin degradation under exposure to HNO_3 vapours. This approach is highly effective for evaluating wood behaviour under acidic conditions that simulate aging. Dynamic mechanical experiments assess the mechanical properties of the wood, such as stiffness and elasticity, which are crucial for determining its usability and durability. The analysis provides a quantitative measure of the treatment effects on the wood's response to stress over time. Monitoring lignin, a key component of wood maintaining its structural integrity, allowed us to observe the chemical breakdown that compromises the strength of aged AW. These methods create a comprehensive evaluation on the long-term effectiveness of treatments from both a chemical and mechanical perspective.

3.6.1. Compression properties of wooden samples before and after aging

Fig. 9a illustrates the stress vs strain curves of AW samples before and after treatment with chitosan solution, and chitosan/HNTs mixtures containing the lowest and largest halloysite contents (0.2 and 3 wt%, respectively). As compared with untreated AW, we observed relevant increases (up to 74 %) of the elastic modulus after the treatment with chitosan/HNTs mixtures suggesting that the filling of wooden channels with clay nanotubes enhances the rigidity of the waterlogged archaeological wood contributing to improve the mechanical performances. On the other hand, the treatement by chitosan solution generated a smaller improvement of the elastic modulus of AW.

As concerns the wooden samples after acidic aging (Fig. 9b), it is confirmed that the archeological woods treated by chitosan/HNTs are more rigid in comparison with the untreated AW, while a decrease of the elastic modulus was detected after treatment with chitosan solution. The latter highlights that chitosan does not improve the mechanical performances of aged wood that can be related to disintegration of the biopolymeric coating layer due to the exposure to acidic vapours. In contrast, the combination of chitosan with HNTs is successful to enhance the mechanical behaviour of AW because clay nanotubes penetrate within the wooden structure acting as reinforcing nanofillers despite the aging conditions. As example, the treatement of chit/HNTs 2 wt% determine an improvement of ca. 32 % for elastic modulus of AW. All the elastic modulus data are collected in Fig. 9c.

Moreover, the stress vs strain curves (Fig. 9a,b) presented a yield point, defined as a morphological turning point between the elastic region and the plateau region that reflects the onset of permanent deformation in the wood structure. Interestingly, the yield point is more evident for untreated AW as compared to treated samples. After the yield point, the wood's cell walls begin to fail, initiating the plastic and densification regions. In these regions, the wood's vessels start to collapse and deform, signifying structural weakness as the material

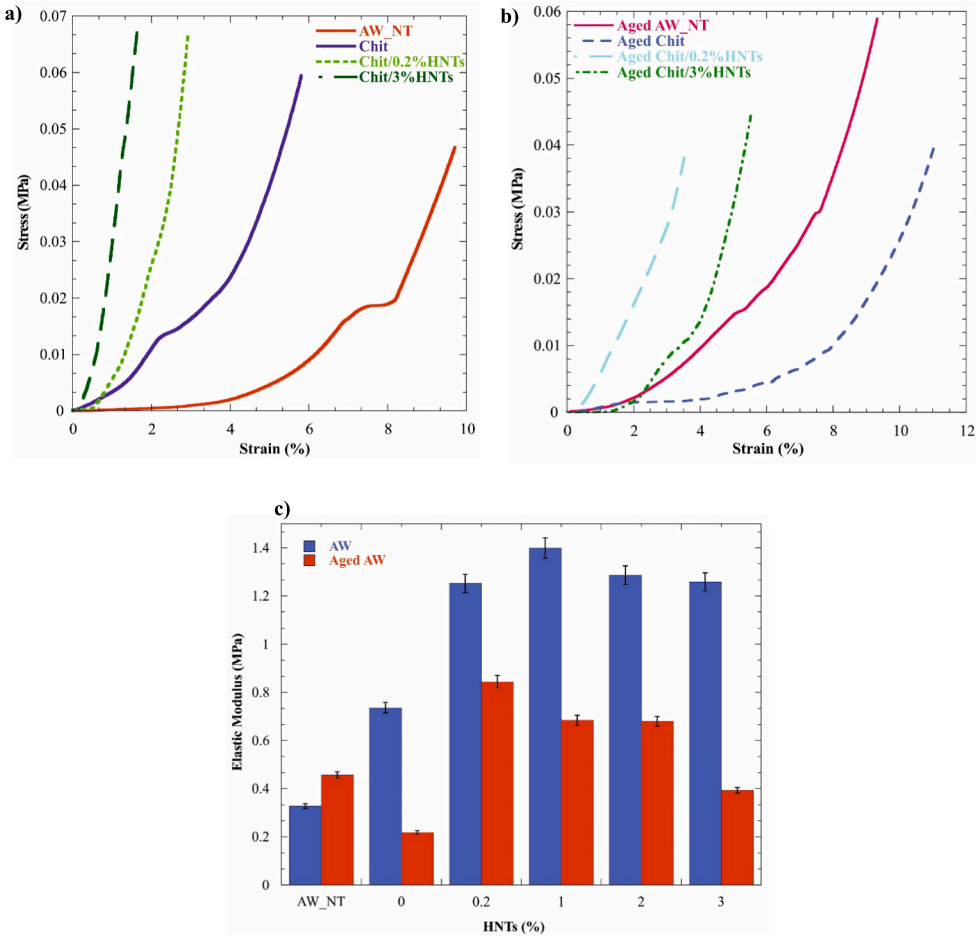

Fig. 9. Stress vs Strain curves of untreated and treated wood samples before (a) and after (b) aging process. c) Elastic Modulus diagram as function of HNTs% of treated and untreated wood samples before and after aging process.

transitions from elastic deformation to plastic flow [75]. In the densification regime [75], where stress rises sharply with increasing strain, we calculated the stress at the breaking point. The results indicate that the stress at the breaking point increases with higher concentrations of HNTs with respect to the untreated wood samples (Tables S3,S4 in Supplementary Materials). This confirms that the addition of HNTs reinforces the wood, allowing it to withstand higher stresses before break. In conclusion, DMA results highlighted that the simultaneous presence of chitosan and HNTs during the immersion protocol improves both the rigidity and the mechanical resistance of waterlogged archaeological wood before and after its acidic aging. Namely, woods treated by chitosan/HNTs mixtures are more resilient to compression forces besides the acidic aggressive conditions.

3.6.2. Effects of aging on the lignin index of untreated and treated woods.

The analysis of the FTIR spectra focuses on evaluating lignin index of untreated and treated wood samples after aging (Fig. S6 in Supplementary Materials). As reported in literature [18], the lignin index (LI) was determined by normalizing the peak intensities of the lignin group at 1511 cm^{-1} with the C—H deformation and CH_3 groups at 1375 cm^{-1}. This normalization provides a reliable metric for assessing the extent of lignin preservation or degradation over time. Upon exposure to HNO_3 vapours, untreated wood showed a significant LI reduction, with a variation of LI (ΔLI) of 99 %, indicating near-complete lignin degradation, underlining lignin's vulnerability, especially in aged AW, where it constitutes a major structural component (Fig. 10). In contrast, all treatments determined lower ΔLI reductions (ca. 60 %) highlighting that the presence of chitosan and HNTs promote the protection of lignin

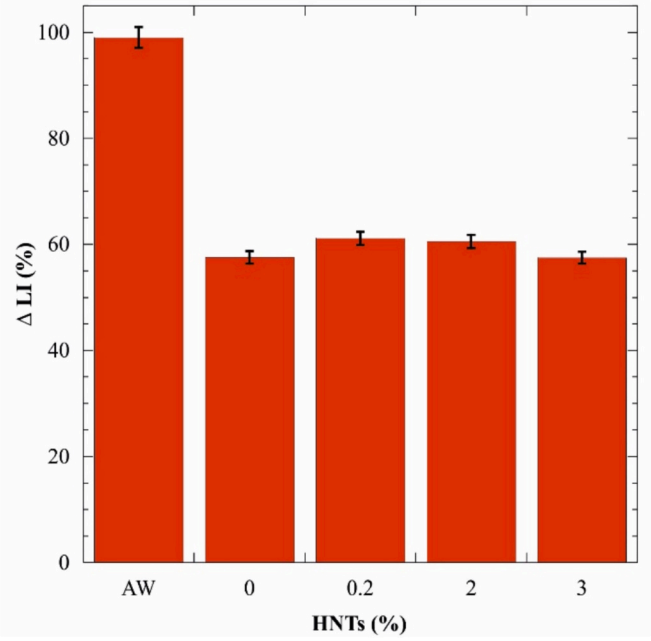

Fig. 10. Variation of the lignin index after wood exposure to HNO_3 vapours. Relative error for variation of lignin index is 2 %.

under oxidative and/or acidic conditions, thereby enhancing wood preservation (Fig. 8). Interestingly, the lignin protection obtained by chitosan/HNTs treatment is better with respect to that determined by AW immersion in aqueous mixtures of PEG1500 and HNTs loaded with $Ca(OH)_2$ that evidenced larger ΔLI values (ca. 80 %) [18].

3.7. Comprehensive description of the influence of chitosan/HNTs on waterlogged archaeological woods

Chitosan and halloysite clay nanotubes possess functional properties that can be perspective for treatment of waterlogged archaeological woods. Specifically, chitosan is antioxidant and antimicrobial biopolymer assuring extended protection for the wooden structure, while HNTs are proper nanofillers for consolidation of AW channels increasing the integrity and mechanical performances of woods. According to these considerations, we employed chitosan/HNTs aqueous mixtures for AW treatment by immersion protocol, which was already used with dispersions of halloysite and polymers, such as beeswax [20] and polyethylene glycol [18], as well as with Pickering emulsions based on paraffin and HNTs [19].

As compared with treatment by pristine chitosan, we detected that mass change upon drying is decreased by adding HNTs to chitosan dispersion. This finding is due to capacity of halloysite clay nanotubes to fill the wooden channels reducing the AW porosity. On the other hand, chitosan mainly created a protective coating layer generating a slight effect on the wood structure. Based on thermogravimetric data, we calculated the amounts of HNTs entrapped within the wood pores. We detected that AW treated with chitosan/HNTs 3 wt% contains a large content (40 w%) of halloysite confirming the excellent consolidation efficiency. Moreover, thermogravimetry evidenced that the thermal degradation of wood components (cellulose and lignin) is shifted to higher temperature after treatment with chitosan/HNTs dispersion. These results can be attributed to barrier effect capacity of clay nanotubes towards the volatile products generated by thermal decomposition of organic macromolecules. Accordingly, we observed that the thermal stabilization effect is stronger by increasing the HNTs amounts filled within the wooden channels. As expected, the hygroscopic behaviour of wood decreased by consolidation treatment with chitosan/HNTs due to reduction of wood porosity. Remarkably, the filling of wood channels improved significantly the mechanical properties of waterlogged archaeological woods. This improvement was observed also in woods aged by HNO_3 vapours highlighting that the combination of chitosan and HNTs is successful to prevent the AW deterioration under acidic conditions. In contrast, the treatment by pristine chitosan did not guarantee mechanical improvements for aged woods because the biopolymeric coating layer can removed by acidic vapours.

4. Conclusions

This study highlights the suitability of chitosan/halloysite aqueous dispersions for the consolidation of waterlogged archaeological woods using an immersion protocol. The treatment efficiency depends on the concentration and distribution of both chitosan and halloysite clay nanotubes (HNTs). The increase of halloysite amount in the consolidating mixture improved the penetration of chitosan within the wooden structure. The consolidation efficiency was enhanced (up to ca. 8 %) by adding HNTs to chitosan dispersion.

Details on the distribution of chitosan and HNTs within the wooden structure were achieved by elemental analysis through ED-XRF demonstrating the uniform incorporation of the consolidants within the archaeological wood.

According to the colorimetric study, small amounts (0.2–2 wt%) of HNTs generated negligible colour changes, while the largest HNTs concentration (3 wt%) caused more significant colorimetric variations affecting the wood appearance. Thermogravimetric analysis indicated that wood treated by 3 wt% HNTs exhibits enhanced thermal stability due to the interactions between chitosan and HNTs. Water uptake tests evidenced that treated woods present lower hygroscopicity than untreated sample in agreement with the lower water vapor absorption capacities. Untreated wood absorbed the largest water amount during immersion tests as expected by its high porosity. A slight reduction of water absorption was observed after wood treatment with pristine chitosan, which forms a protective coating layer. The addition of HNTs to chitosan dispersion improved water resistance of treated wood because of the encapsulation of clay nanotubes within the wooden structure.

Moreover, the filling with HNTs improved the compression properties (especially the elastic modulus) of the chitosan treated wood. Untreated wood exhibited structural weaknesses, while treated wood showed better resistance to compression with the elastic modulus. The wood treated with chitosan/HNTs 2 wt% exhibited an elastic modulus of 0.6847 MPa demonstrating significant mechanical reinforcement.

HNTs provided greater mechanical stability compared to pristine chitosan, which did not notably enhance the properties of aged wood. Regarding lignin degradation, untreated wood showed a 99 % reduction in the lignin index (LI) after exposure to HNO_3 vapours, indicating complete wood degradation. Chitosan treatment reduced this degradation to 57 %, forming a protective barrier on wood surface. Similar results were detected for woods treated with chitosan/HNTs dispersions.

In conclusion, the treatment by chitosan/HNTs aqueous mixtures improved both mechanical properties and water resistance of waterlogged archaeological woods contributing to lignin preservation upon acidic aging. This combination offers a promising approach for the long-term stabilization of aged wood, balancing mechanical strength and chemical protection.

CRediT authorship contribution statement

Maria Rita Caruso: Writing – original draft, Investigation, Formal analysis, Data curation. **Giulia D'Agostino:** Investigation, Data curation. **Giuseppe Cavallaro:** Writing – review & editing, Validation, Supervision, Conceptualization. **Olivia Gómez-Laserna:** Validation, Conceptualization. **Maite Maguregui:** Writing – review & editing, Supervision, Funding acquisition. **Giuseppe Lazzara:** Writing – review & editing, Funding acquisition, Conceptualization.

Declaration of competing interest

The authors declare that they have no known competing financial interests or personal relationships that could have appeared to influence the work reported in this paper.

Acknowledgements

This work has been supported by grant TED2021-129299A-I00, funded by MICIU/AEI/10.13039/501100011033 and by the European Union NextGenerationEU/PRTR and by PON "Research and Innovation" 2014-2020, Asse IV "Istruzione e ricerca per il recupero", all'Azione IV.5 "Dottorati su tematiche green". DM 1061/2021 and by the University of Palermo.

Appendix A. Supplementary data

Supplementary data to this article can be found online at https://doi.org/10.1016/j.ijbiomac.2025.147126.

Data availability

Data will be made available on request.

References

[1] M.R. Caruso, G. Cavallaro, S. Milioto, G. Lazzara, Halloysite nanotubes/Keratin composites for wool treatment, Appl. Clay Sci. 238 (2023) 106930, https://doi.org/10.1016/j.clay.2023.106930.

[2] G. D'Agostino, M.R. Caruso, G. Cavallaro, G. Lazzara, S. Milioto, Pickering emulsion gel based on Funori biopolymer and Halloysite nanotubes: a new sustainable material for the cleaning of artwork surfaces, ACS Appl. Polym. Mater. 6 (2024) 7679–7690, https://doi.org/10.1021/acsapm.4c01152.

[3] S. Franco, L. Severini, E. Buratti, L. Tavagnacco, S. Sennato, L. Micheli, M. Missori, B. Ruzicka, C. Mazzuca, E. Zaccarelli, R. Angelini, Gellan-based hydrogels and microgels: a rheological perspective, Carbohydr. Polym. 354 (2025) 123329, https://doi.org/10.1016/j.carbpol.2025.123329.

[4] C. Goudenhooft, A. Melelli, S. Durand, X. Falourd, L. Le-Bot, L. Morgillo, S. Gaballah, R. Cortopassi, A. Quiles, D.U. Shah, F. Jamme, J. Beaugrand, A. Bourmaud, Comparison of kink-band structures and specificities of cell wall polysaccharides in modern and ancient flax fibres, Carbohydr. Polym. 344 (2024) 122526, https://doi.org/10.1016/j.carbpol.2024.122526.

[5] D. Bandelli, R. Mastrangelo, G. Poggi, D. Chelazzi, P. Baglioni, New sustainable polymers and oligomers for Cultural Heritage conservation, Chem. Sci. 15 (2024) 2443–2455, https://doi.org/10.1039/D3SC03909A.

[6] M.R. Caruso, G. D'Agostino, S. Milioto, G. Cavallaro, G. Lazzara, A review on biopolymer-based treatments for consolidation and surface protection of cultural heritage materials, J. Mater. Sci. 58 (2023) 12954–12975, https://doi.org/10.1007/s10853-023-08833-5.

[7] A.P. Kanth, A.K. Soni, Application of nanocomposites for conservation of materials of cultural heritage, J. Cult. Herit. 59 (2023) 120–130, https://doi.org/10.1016/j.culher.2022.11.010.

[8] P.R. Yaashikaa, P. Senthil Kumar, S. Karishma, Review on biopolymers and composites – Evolving material as adsorbents in removal of environmental pollutants, Environ. Res. 212 (2022) 113114, https://doi.org/10.1016/j.envres.2022.113114.

[9] G. Cavallaro, G. Lazzara, F. Parisi, S. Riela, S. Milioto, Nanoclays for Conservation, in: Nanotechnologies Nanomater. Diagn. Conserv. Restor. Cult. Herit., Elsevier, 2019, pp. 149–170, https://doi.org/10.1016/B978-0-12-813910-3.00008-2.

[10] M. Broda, C.A.S. Hill, Conservation of waterlogged wood—past, present and future perspectives, Forests 12 (2021) 1193, https://doi.org/10.3390/f12091193.

[11] W. Yang, W. Ma, X. Liu, Evaluation of deterioration degree of archaeological wood from Luoyang Canal No. 1 ancient ship, Forests 15 (2024) 963, https://doi.org/10.3390/f15060963.

[12] Z. Walsh-Korb, Sustainability in Heritage Wood Conservation: Challenges and Directions for Future Research, Forests 13 (2021) 18, https://doi.org/10.3390/f13010018.

[13] M. Broda, J.E. Jakes, L. Li, O.A. Antipova, Archeological wood conservation with selected organosilicon compounds studied by XFM and nanoindentation, Wood Sci. Technol. 57 (2023) 1277–1298, https://doi.org/10.1007/s00226-023-01503-4.

[14] P. Kryg, B. Mazela, W. Perdoch, M. Broda, Challenges and prospects of applying nanocellulose for the conservation of wooden cultural heritage—a review, Forests 15 (2024) 1174, https://doi.org/10.3390/f15071174.

[15] Z. Walsh-Korb, I. Stelzner, J. Dos Santos Gabriel, G. Eggert, L. Avérous, Morphological study of bio-based polymers in the consolidation of waterlogged wooden objects, Materials 15 (2022) 681, https://doi.org/10.3390/ma15020681.

[16] X. Liu, X. Tu, W. Ma, C. Zhang, H. Huang, A.M. Varodi, Consolidation and dehydration of waterlogged archaeological wood from Site Huaguangjiao No.1, Forests 13 (2022) 1919, https://doi.org/10.3390/f13111919.

[17] Z. Walsh, E.-R. Janeček, J.T. Hodgkinson, J. Sedlmair, A. Koutsioubas, D.R. Spring, M. Welch, C.J. Hirschmugl, C. Toprakcioglu, J.R. Nitschke, M. Jones, O. A. Scherman, Multifunctional supramolecular polymer networks as next-generation consolidants for archaeological wood conservation, Proc. Natl. Acad. Sci. 111 (2014) 17743–17748, https://doi.org/10.1073/pnas.1406037111.

[18] G. Cavallaro, S. Milioto, F. Parisi, G. Lazzara, Halloysite nanotubes loaded with calcium hydroxide: alkaline fillers for the deacidification of waterlogged archeological woods, ACS Appl. Mater. Interfaces 10 (2018) 27355–27364, https://doi.org/10.1021/acsami.8b09416.

[19] L. Lisuzzo, T. Hueckel, G. Cavallaro, S. Sacanna, G. Lazzara, Pickering emulsions based on wax and halloysite nanotubes: an ecofriendly protocol for the treatment of archeological woods, ACS Appl. Mater. Interfaces 13 (2021) 1651–1661, https://doi.org/10.1021/acsami.0c20443.

[20] G. Cavallaro, G. Lazzara, S. Milioto, F. Parisi, V. Sparacino, Thermal and dynamic mechanical properties of beeswax-halloysite nanocomposites for consolidating waterlogged archaeological woods, Polym. Degrad. Stab. 120 (2015) 220–225, https://doi.org/10.1016/j.polymdegradstab. 2015.07.007.

[21] F. Antonelli, G. Galotta, G. Sidoti, F. Zikeli, R. Nisi, B. Davidde Petriaggi, M. Romagnoli, Cellulose and lignin nano-scale consolidants for waterlogged archaeological wood, Front. Chem. 8 (2020) 32, https://doi.org/10.3389/fchem.2020.00032.

[22] Y. Feng, X. Chen, R.-R. He, Z. Liu, Y.M. Lvov, M. Liu, The horizons of medical mineralogy: structure-bioactivity relationship and biomedical applications of halloysite nanoclay, ACS Nano 18 (2024) 20001–20026, https://doi.org/10.1021/acsnano.4c04372.

[23] A. Stavitskaya, E. Khusnetdenova, V. Vinokurov, Y. Lvov, R. Fakhrullin, Prokaryotic and eukaryotic toxicity of halloysite decorated with photoactive nanoparticles, Chem. Commun. 58 (2022) 7719–7729, https://doi.org/10.1039/D2CC02439J.

[24] M. alleshagh, S. Sadjadi, H. Arabi, N. Bahri-Laleh, E. Monflier, Palladated chitosan-halloysite bead as an efficient catalyst for hydrogenation of lubricants, Mater. Chem. Phys. 278 (2022) 125506, https://doi.org/10.1016/j.matchemphys.2021.125506.

[25] Y. Feng, X. Zhou, J. Yang, X. Gao, L. Yin, Y. Zhao, B. Zhang, Encapsulation of ammonia borane in Pd/halloysite nanotubes for efficient thermal dehydrogenation, ACS Sustain. Chem. Eng. 8 (2020) 2122–2129, https://doi.org/10.1021/acssuschemeng.9b04480.

[26] S. Sadjadi, M.M. Heravi, S.S. Kazemi, Ionic liquid decorated chitosan hybridized with clay: a novel support for immobilizing Pd nanoparticles, Carbohydr. Polym. 200 (2018) 183–190, https://doi.org/10.1016/j.carbpol.2018.07.093.

[27] Y. Zhao, S. Guo, X. Xue, C. Xiong, X. Gao, B. Zhang, Halloysite nanotubes supported Co2P bridged by carbon dots for enhanced hydrogen evolution from ammonia borane, Chem. Eng. J. 483 (2024) 149332, https://doi.org/10.1016/j.cej.2024.149332.

[28] E. Boccalon, G. Viscusi, E. Lamberti, F. Fancello, S. Zara, P. Sassi, M. Marinozzi, M. Nocchetti, G. Gorrasi, Composite films containing red onion skin extract as intelligent pH indicators for food packaging, Appl. Surf. Sci. 593 (2022) 153319, https://doi.org/10.1016/j.apsusc.2022.153319.

[29] G. Viscusi, V. Bugatti, G. Gorrasi, Active packaging based on cellulose trays coated with layered double hydroxide as nano-carrier of parahydroxybenzoate: application to fresh-cut iceberg lettuce, Packag. Technol. Sci. 34 (2021) 353–360, https://doi.org/10.1002/pts.2565.

[30] M.R. Caruso, M.M. Calvino, P. Šiler, L. Cába, S. Milioto, L. Lisuzzo, G. Lazzara, G. Cavallaro, Self-standing biohybrid xerogels incorporating nanotubular clays for sustainable removal of pollutants, Small 21 (2025) 2405215, https://doi.org/10.1002/smll.202405215.

[31] M. Fizir, A. Richa, S. Touil, Y. Benmokadem, K. Boubekeur, B. Hallal, H. Drici, L. Wei, Preparation and application of a surfactant-modified Halloysite nanotubes for the adsorption of nitrates from aqueous solutions: kinetic and equilibrium studies, Environ. Prog. Sustain. Energy 42 (2023) e13995, https://doi.org/10.1002/ep.13995.

[32] O. Owoseni, Y. Su, S. Raghavan, A. Bose, V.T. John, Hydrophobically modified chitosan biopolymer connects halloysite nanotubes at the oil-water interface as complementary pair for stabilizing oil droplets, J. Colloid Interface Sci. 620 (2022) 135–143, https://doi.org/10.1016/j.jcis.2022.03.142.

[33] A. Panchal, L.T. Swientoniewski, M. Omarova, T. Yu, D. Zhang, D.A. Blake, V. John, Y.M. Lvov, Bacterial proliferation on clay nanotube Pickering emulsions for oil spill bioremediation, Colloids Surf. B: Biointerfaces 164 (2018) 27–33, https://doi.org/10.1016/j.colsurfb.2018.01.021.

[34] X. Tang, G.I. Urujeni, X. Ni, Z. Lu, D. Wang, J. Gao, F. Meriem, H. He, D. Xiao, P. Dramou, Polyethyleneimine in designed nanocomposite based magnetic halloysite nanotubes for extraction and determination of gallic acid in green tea, Int. J. Biol. Macromol. 265 (2024) 130914, https://doi.org/10.1016/j.ijbiomac.2024.130914.

[35] Y. Feng, X. Luo, Z. Li, X. Fan, Y. Wang, R.-R. He, M. Liu, A ferroptosis-targeting ceria anchored halloysite as orally drug delivery system for radiation colitis therapy, Nat. Commun. 14 (2023) 5083, https://doi.org/10.1038/s41467-023-40794-w.

[36] M. Liu, R. Fakhrullin, A. Novikov, A. Panchal, Y. Lvov, Tubule nanoclay-organic heterostructures for biomedical applications, Macromol. Biosci. 19 (2019) 1800419, https://doi.org/10.1002/mabi.201800419.

[37] M. Liu, R. Fakhrullin, A. Stavitskaya, V. Vinokurov, N. Lama, Y. Lvov, Micropatterning of biologically derived surfaces with functional clay nanotubes, Sci. Technol. Adv. Mater. 25 (2024) 2327276, https://doi.org/10.1080/14686996.2024.2327276.

[38] Q. Li, X. Hu, P. Perkins, T. Ren, Antimicrobial film based on poly(lactic acid) and natural halloysite nanotubes for controlled cinnamaldehyde release, Int. J. Biol. Macromol. 224 (2023) 848–857, https://doi.org/10.1016/j.ijbiomac.2022.10.171.

[39] G. Cavallaro, G. Lazzara, S. Milioto, Nanocomposites based on halloysite nanotubes and sulphated galactan from red seaweed Gloiopeltis: Properties and delivery capacity of sodium diclofenac, Int. J. Biol. Macromol. 234 (2023) 123645, https://doi.org/10.1016/j.ijbiomac.2023.123645.

[40] F. Kazemi-Aghdam, V. Jahed, M. Dehghan-Niri, F. Ganji, E. Vasheghani-Farahani, Injectable chitosan hydrogel embedding modified halloysite nanotubes for bone tissue engineering, Carbohydr. Polym. 269 (2021) 118311, https://doi.org/10.1016/j.carbpol.2021.118311.

[41] M. Liu, C. Wu, Y. Jiao, S. Xiong, C. Zhou, Chitosan–halloysite nanotubes nanocomposite scaffolds for tissue engineering, J. Mater. Chem. B 1 (2013) 2078–2089, https://doi.org/10.1039/C3TB20084A.

[42] Y. Wang, S. Yi, R. Lu, D.E. Sameen, S. Ahmed, J. Dai, W. Qin, S. Li, Y. Liu, Preparation, characterization, and 3D printing verification of chitosan/halloysite nanotubes/tea polyphenol nanocomposite films, Int. J. Biol. Macromol. 166 (2021) 32–44, https://doi.org/10.1016/j.ijbiomac.2020.09.253.

[43] P. Dramou, M. Fizir, A. Taleb, A. Itatahine, N.S. Dahiru, Y.A. Mehdi, L. Wei, J. Zhang, H. He, Folic acid-conjugated chitosan oligosaccharide-magnetic halloysite nanotubes as a delivery system for camptothecin, Carbohydr. Polym. 197 (2018) 117–127, https://doi.org/10.1016/j.carbpol.2018.05.071.

[44] A. Paul, R. Augustine, A. Hasan, A.A. Zahid, S. Thomas, C. Agatemor, K. Ghosal, Halloysite nanotube and chitosan polymer composites: physicochemical and drug delivery properties, J. Drug Deliv. Sci. Technol. 72 (2022) 103380, https://doi.org/10.1016/j.jddst.2022.103380.

[45] M. Barman, S. Mahmood, R. Augustine, A. Hasan, S. Thomas, K. Ghosal, Natural halloysite nanotubes /chitosan based bio-nanocomposite for delivering norfloxacin, an anti-microbial agent in sustained release manner, Int. J. Biol. Macromol. 162 (2020) 1849–1861, https://doi.org/10.1016/j.ijbiomac.2020.08.060.

[46] M.R. Caruso, G. D'Agostino, J. Wasserbauer, P. Šiler, G. Cavallaro, S. Milioto, G. Lazzara, Filling of chitosan film with wax/halloysite microparticles for absorption of hydrocarbon vapors, Adv. Sustain. Syst. 8 (2024) 2400026, https://doi.org/10.1002/adsu.202400026.
[47] Q. Li, Y. Hu, B. Zhang, Polyoxometalate-Ionic Liquids (ILs) and polyvinyl alcohol/chitosan/ILs hydrogels for inhibiting bacteria colonising wall paintings, Carbohydr. Polym. 256 (2021) 117592, https://doi.org/10.1016/j.carbpol.2020.117592.
[48] D. Ailincai, M. Bercea, I. Rosca, I.A. Sandu, L. Marin, Antimicrobial chitosan-based hydrogels: a novel approach to obtain sanitizers, Carbohydr. Polym. 354 (2025) 123288, https://doi.org/10.1016/j.carbpol.2025.123288.
[49] Z. Liao, J. Li, W. Ni, R. Zhan, X. Xu, Co-delivery of antimicrobial peptide and Prussian blue nanoparticles by chitosan/polyvinyl alcohol hydrogels, Carbohydr. Polym. 348 (2025) 122873, https://doi.org/10.1016/j.carbpol.2024.122873.
[50] F. Zhang, S. Zhang, S. Cui, X. Jing, Y. Feng, S. Coseri, Rapid self-healing carboxymethyl chitosan/hyaluronic acid hydrogels with injectable ability for drug delivery, Carbohydr. Polym. 328 (2024) 121707, https://doi.org/10.1016/j.carbpol.2023.121707.
[51] A. Zając, J. Hanuza, M. Wandas, L. Dymińska, Determination of N-acetylation degree in chitosan using Raman spectroscopy, Spectrochim. Acta A Mol. Biomol. Spectrosc. 134 (2015) 114–120, https://doi.org/10.1016/j.saa.2014.06.071.
[52] M.R. Caruso, M.M. Calvino, P. Šiler, L. Cába, S. Milioto, L. Lisuzzo, G. Lazzara, G. Cavallaro, Self-standing biohybrid xerogels incorporating nanotubular clays for sustainable removal of pollutants, Small 21 (2025) 2405215, https://doi.org/10.1002/smll.202405215.
[53] D.I. Donato, G. Lazzara, S. Milioto, Thermogravimetric analysis, J. Therm. Anal. Calorim. 101 (2010) 1085–1091, https://doi.org/10.1007/s10973-010-0717-9.
[54] I.D. Donato, G. Lazzara, Porosity Determination with Helium Pycnometry as a method to characterize waterlogged woods and the efficacy of the consolidation treatments, Archaeometry 54 (2012) 906–915, https://doi.org/10.1111/j.1475-4754.2011.00657.x.
[55] G. Cavallaro, D.I. Donato, G. Lazzara, S. Milioto, A comparative thermogravimetric study of waterlogged archaeological and sound woods, J. Therm. Anal. Calorim. 104 (2011) 451–457, https://doi.org/10.1007/s10973-010-1229-3.
[56] N. Macchioni, E. Pecoraro, B. Pizzo, The measurement of maximum water content (MWC) on waterlogged archaeological wood: a comparison between three different methodologies, J. Cult. Herit. 30 (2018) 51–56, https://doi.org/10.1016/j.culher.2017.10.005.
[57] N. Macchioni, C. Capretti, L. Sozzi, B. Pizzo, Grading the decay of waterlogged archaeological wood according to anatomical characterisation. The case of the Fiavé site (N-E Italy), Int. Biodeterior. Biodegrad. 84 (2013) 54–64, https://doi.org/10.1016/j.ibiod.2013.05.028.
[58] G. Cavallaro, M.R. Caruso, S. Milioto, R. Fakhrullin, G. Lazzara, Keratin/alginate hybrid hydrogels filled with halloysite clay nanotubes for protective treatment of human hair, Int. J. Biol. Macromol. 222 (2022) 228–238, https://doi.org/10.1016/j.ijbiomac.2022.09.170.
[59] E. Calparsoro, M. Maguregui, H. Morillas, G. Arana, J.G. Iñañez, Non-destructive screening methodology based on ED-XRF for the classification of medieval and post-medieval archaeological ceramics, Ceram. Int. 45 (2019) 10672–10683, https://doi.org/10.1016/j.ceramint.2019.02.138.
[60] C. García-Florentino, M. Maguregui, J.A. Carrero, H. Morillas, G. Arana, J. M. Madariaga, Development of a cost effective passive sampler to quantify the particulate matter depositions on building materials over time, J. Clean. Prod. 268 (2020) 122134, https://doi.org/10.1016/j.jclepro.2020.122134.
[61] I. Marcaida, M. Maguregui, H. Morillas, S. Perez-Diez, J.M. Madariaga, Raman imaging to quantify the thermal transformation degree of Pompeian yellow ochre caused by the 79 AD Mount Vesuvius eruption, Anal. Bioanal. Chem. 411 (2019) 7585–7593, https://doi.org/10.1007/s00216-019-02175-5.
[62] H. Morillas, F.F. de Mendonça Filho, H. Derluyn, M. Maguregui, D. Grégoire, J. M. Madariaga, Decay processes in buildings close to the sea induced by marine aerosol: Salt depositions inside construction materials, Sci. Total Environ. 721 (2020) 137687, https://doi.org/10.1016/j.scitotenv.2020.137687.
[63] M. Romagnoli, G. Galotta, F. Antonelli, G. Sidoti, M. Humar, D. Kržišnik, K. Čufar, B. Davidde Petriaggi, Micro-morphological, physical and thermogravimetric analyses of waterlogged archaeological wood from the prehistoric village of Gran Carro (Lake Bolsena-Italy), Cult. Herit. Times Armed Confl. Middle East Much More Mater. Damage 33 (2018) 30–38, https://doi.org/10.1016/j.culher.2018.03.012.
[64] K.E. High, K.E.H. Penkman, A review of analytical methods for assessing preservation in waterlogged archaeological wood and their application in practice, Herit. Sci. 8 (2020) 83, https://doi.org/10.1186/s40494-020-00422-y.
[65] A. Lo Bianco, M.M. Calvino, G. Cavallaro, L. Lisuzzo, P. Pasbakhsh, S. Milioto, G. Lazzara, Y. Lvov, Flame-resistant inorganic films by self-assembly of clay nanotubes and their conversion to geopolymer for CO2 capture, Small 20 (2024) 2406812, https://doi.org/10.1002/smll.202406812.
[66] M. Zborowska, P. Niedzielski, A. Budka, J. Enenche, M. Mleczek, Content of elements in contemporary and archaeological wood as a marker of possible change in physico-chemical parameters, J. Cult. Herit. 63 (2023) 90–100, https://doi.org/10.1016/j.culher.2023.07.011.
[67] M. Broda, B. Mazela, K. Krolikowska-Pataraja, C.S.A. Hill, The use of FT-IR and computed tomography non-destructive technique for waterlogged wood characterisation, Wood Res. 60 (2015) 707–722.
[68] M. Ziegler-Borowska, D. Chełminiak, H. Kaczmarek, Thermal stability of magnetic nanoparticles coated by blends of modified chitosan and poly(quaternary ammonium) salt, J. Therm. Anal. Calorim. 119 (2015) 499–506, https://doi.org/10.1007/s10973-014-4122-7.
[69] I. Corazzari, R. Nisticò, F. Turci, M.G. Faga, F. Franzoso, S. Tabasso, G. Magnacca, Advanced physico-chemical characterization of chitosan by means of TGA coupled on-line with FTIR and GCMS: Thermal degradation and water adsorption capacity, Polym. Degrad. Stab. 112 (2015) 1–9, https://doi.org/10.1016/j.polymdegradstab. 2014.12.006.
[70] E. González-Díaz, J.-M. Alonso-López, Characterization by thermogravimetric analysis of the wood used in Canary architectural heritage, J. Cult. Herit. 23 (2017) 111–118, https://doi.org/10.1016/j.culher.2016.09.002.
[71] D. Shen, X. Gu, H. Zhang, N. Macchioni, Q. Cheng, X. Tian, J. Du, N. Li, K. Yuan, Study on the feasibility of the TG method for maximum water content measurement of waterlogged archaeological wood, Stud. Conserv. 69 (2024) 621–634, https://doi.org/10.1080/00393630.2023.2278358.
[72] M. Fahimizadeh, L.W. Wong, Z. Baifa, S. Sadjadi, S.A.B. Auckloo, K. Palaniandy, P. Pasbakhsh, J.B.L. Tan, R.K.R. Singh, P. Yuan, Halloysite clay nanotubes: Innovative applications by smart systems, Appl. Clay Sci. 251 (2024) 107319, https://doi.org/10.1016/j.clay.2024.107319.
[73] G. Gorrasi, Dispersion of halloysite loaded with natural antimicrobials into pectins: characterization and controlled release analysis, Carbohydr. Polym. 127 (2015) 47–53, https://doi.org/10.1016/j.carbpol.2015.03.050.
[74] S. Gaurav (Ed.), Digital Color Imaging Handbook, 1st ed., CRC Press, 2017 https://doi.org/10.1201/9781420041484.
[75] C. Huang, M. Gong, Y. Chui, F. Chan, Mechanical behaviour of wood compressed in radial direction-part I. New method of determining the yield stress of wood on the stress-strain curve, J. Bioresour. Bioprod. 5 (2020) 186–195, https://doi.org/10.1016/j.jobab.2020.07.004.